Monoclinic zinc monotungstate Yb^{3+},Li^{+}:$ZnWO_4$: Part I. Czochralski growth, structure refinement and Raman spectra

Kirill Subbotin[a,b], Pavel Loiko[c], Sami Slimi[d,f], Anna Volokitina[d,e], Anatoly Titov[a,b], Denis Lis[a], Elena Chernova[a], Sergei Kuznetsov[a], Rosa Maria Solé[d], Uwe Griebner[g], Valentin Petrov[g], Magdalena Aguiló[d], Francesc Díaz[d], Patrice Camy[c], Evgenii Zharikov[a] and Xavier Mateos[d,*]

[a]*Prokhorov General Physics Institute, Russian Academy of Sciences, 38 Vavilova St., 119991 Moscow, Russia*
[b]*Mendeleev University of Chemical Technology of Russia, 9 Miusskaya Sq., 125047 Moscow, Russia*
[c]*Centre de Recherche sur les Ions, les Matériaux et la Photonique (CIMAP), UMR 6252 CEA-CNRS-ENSICAEN, Université de Caen Normandie, 6 Boulevard du Maréchal Juin, 14050 Caen Cedex 4, France*
[d]*Universitat Rovira i Virgili (URV), Física i Cristal·lografia de Materials i Nanomaterials (FiCMA-FiCNA)-EMaS, Marcel.li Domingo 1, 43007 Tarragona, Spain*
[e]*I.P.E.I. of Monastir, Unit of Materials and Organic Synthesis UR17ES31, 5019 Monastir, Tunisia*
[f]*ITMO University, Kronverkskiy Pr., 49, 197101 Saint-Petersburg, Russia*
[g]*Max Born Institute for Nonlinear Optics and Short Pulse Spectroscopy, Max-Born-Str. 2a, 12489 Berlin, Germany*
**Corresponding author, e-mail: xavier.mateos@urv.cat*

Abstract. We report on the growth of a co-doped divalent-metal monotungstate crystal, Yb^{3+},Li^{+}:$ZnWO_4$, its structure refinement, thermo-mechanical properties and polarized Raman spectra. Yb^{3+},Li^{+}:$ZnWO_4$ crystals are grown by the Czochralski method using Pt/Rh and Pt crucibles. The nature of crystal coloration is discussed and assigned to color centres based on oxygen vacancies as well as Fe^{2+}(Fe^{3+}) species and, possibly, other uncontrolled impurities of transition metal ions. Oxidizing annealing at 800 °C helps to improve the transparency of Yb^{3+},Li^{+}:$ZnWO_4$ leading to a weak residual pink coloration. Yb^{3+},Li^{+}:$ZnWO_4$ was confirmed to be monoclinic (sp. gr. $P2/c$ – C^4_{2h}, No. 13) with lattice constants a = 4.702(2) Å, b = 5.718(6) Å, c = 4.930(4) Å and β = 90.713(5)°. The coefficients of linear thermal expansion are $\alpha_{[100]}$ = 11.71, $\alpha_{[010]}$ = 9.90 and $\alpha_{[001]}$ = 7.01 [10^{-6} K^{-1}]. The melting point of the crystal is at 1166 °C and no thermal effects are found below the melting point. The Yb^{3+},Li^{+}:$ZnWO_4$ crystal shows intense and strongly polarized Raman spectra with the most intense mode at 906.0 cm^{-1} assigned to the W – O stretching vibrations in the [WO_6] octahedra. It is thus a promising gain medium for laser emission at ~1 μm and for self-Raman frequency conversion.

Keywords: tungstate crystals; Czochralski method; impurities; crystal structure; ytterbium lasers; stimulated Raman scattering, coloration.

1. Introduction

The crystal family of monoclinic divalent-metal monotungstates $M^{2+}WO_4$ (where M = Mg, Zn, Cd, *etc*.) is attracting a lot of attention in recent years for optical applications [1-5]. These compounds possess the so-called wolframite [(Fe,Mn)WO_4] type structure belonging monoclinic crystal class, sp. gr. *P*2/*c* [6]. The $M^{2+}WO_4$ crystals are ordered and exhibit a single crystallographic site for the M^{2+} cations with a VI-fold oxygen coordination (site symmetry: C_2) [7]. Two promising examples of this crystal family are magnesium monotungstate ($MgWO_4$, called huanzalaite in the natural mineral form) and zinc monotungstate ($ZnWO_4$, or sanmartinite).

Undoped $M^{2+}WO_4$ crystals and, in particular, $MgWO_4$ and $ZnWO_4$, are known as scintillators [8-11]. $ZnWO_4$ exhibits a relatively wide transmission range (for oxide crystals) of 0.3-5.5 μm, a broad bandgap (~4.5 eV) and an intense luminescence at ~480 nm with a relatively high quantum yield comparable with that for $CdWO_4$ [10]. As a result, $ZnWO_4$ crystals are promising for low-counting experiments to search for double beta (2β) decay, dark matter and also to study rare alpha (α) and beta (β) decays [12,13]. From the point of view of the thermo-mechanical properties, the $MgWO_4$ and $ZnWO_4$ crystals are also attractive because they possess weak anisotropy of thermal expansion [5], satisfactory thermal conductivity κ [14,15] and attractive elastic properties. For example, the thermal conductivity of undoped $ZnWO_4$ at room temperature along the crystallographic axes is $\kappa_{[100]}$ = 4.76, $\kappa_{[010]}$ = 3.17 and $\kappa_{[001]}$ = 4.54 $Wm^{-1}K^{-1}$ [15].

Thanks to these attractive optical and thermal properties, the $MgWO_4$ and $ZnWO_4$ crystals were considered for doping with transition-metal (TM) and rare-earth (RE) ions with the goal of laser operation. Up to now, laser operation was achieved with $MgWO_4$ crystals doped with Yb^{3+} (at ~1 μm) [3,16], Tm^{3+} [17,18] and Ho^{3+} [5] ions (both at ~2 μm), as well as with $ZnWO_4$ crystals doped with Yb^{3+} (at ~1 μm) [19], Tm^{3+} (at ~2 μm) [20] and Dy^{3+} ions (at ~0.58 μm) [21]. These studies revealed some advantageous spectroscopic properties of RE^{3+}-doped $M^{2+}WO_4$ crystals, such as large values and strong anisotropy of transition cross-sections with polarized light, relatively high Stark splitting of the ground states of RE^{3+}-dopants, as well as inhomogeneous broadening of the spectral bands. These features originate from the low-symmetry of the RE^{3+} site (the dopant ions replace for the M^{2+} host-forming cations) and the difference in the ionic radius and valence state of the dopant and the host-forming cations leading to distortion of the local crystal field [22]. A key role of the charge compensation mechanism, presumably involving monovalent alkali-metal cations (e.g., Na^+ from the flux in the case of $MgWO_4$) for the spectroscopic properties of the crystals was also suggested [5,22].

The Yb^{3+}:$MgWO_4$ crystals for 1-μm lasers were grown by the Top Seeded Growth (TSSG) method (from the flux) [3]. Polarized optical spectroscopy and highly-efficient laser operation were reported in [16]. Unlike $MgWO_4$, its zinc counterpart melts congruently at 1188 °C [23] without any polymorphic phase transitions below the melting point, and thus large $ZnWO_4$ crystals can be easily grown from melt by the conventional Czochralski (Cz)

method [24-26]. Yang reported on the Cz growth of Yb^{3+}:$ZnWO_4$ and briefly on its spectroscopic characterization and first laser operation [19].

Despite the growth of undoped $ZnWO_4$ crystals is well documented [24,26], the information about the growth, coloration, doping mechanism, and structure of Yb^{3+}-doped crystals is scarce. Moreover, the use of charge compensators for Yb^{3+}-doped $ZnWO_4$ was not studied so far. On the other hand, it is known from the early studies that the $ZnWO_4$ crystals may exhibit a notable coloration (ranging from almost colorless to pink and black) affecting their optical properties [24,27,28]. It is clear that the color centers and defects may also play a key role in preventing the desired laser operation in Yb^{3+}-doped $ZnWO_4$ crystals. In the present work, we report, for the first time, to the best of our knowledge, on Cz growth of Yb^{3+},Li^+-co-doped $ZnWO_4$ crystals, as well as on a detailed study of the nature of their coloration and the ways of removing them, Yb^{3+} doping, structure refinement, thermal expansion and polarized Raman spectra. The parallel paper [29] is dedicated to the polarization-resolved spectroscopy of Yb^{3+} ions and first laser operation.

To ensure the charge compensation (the Yb^{3+} ions replace for the Zn^{2+} ones, so that the doping is heterovalent), the crystals were co-doped with monovalent lithium cations (Li^+). The use of monovalent alkali-metal cations in crystals with a heterovalent doping is well documented [30,31].

2. Experimental

2.1. Equipment for the crystal growth

Yb^{3+},Li^+:$ZnWO_4$ single crystals were grown by the Cz method at the "Kristall-2" (former USSR) industrial growth facility at Prokhorov General Physics Institute. The growth was performed in air in Pt/Rh or Pt crucibles with a diameter of 30 mm and a height of 30 mm. The pulling rate was 1 mm/h and the rotation speed was 6 rpm. The first undoped single-crystal was obtained by spontaneous nucleation on an Ir wire, so that the growth direction was spontaneous. The seeds for the following growth runs of co-doped crystals were cut from this crystal parallel to the crystallographic plane (010). It is the easiest cleavage plane of $ZnWO_4$. After completing the growth process and separating the crystal from the melt, it was slowly cooled (at a rate of 8 K/h) down to room temperature (RT) in order to avoid cracking.

To prepare the charge for the crystal growth, we used the following reagents: WO_3, ZnO, Li_2CO_3 (as a source of Li^+ ions) and Yb_2O_3 (source of Yb^{3+} ions). WO_3 and ZnO were weighted according to the molar ratio 1:1 with an accuracy of ±0.01 g. The amounts of Yb^{3+} and Li^+ dopant ions were calculated assuming the substitution of the equimolar amounts of Zn^{2+} in the crystal. In particular, we prepared charge compositions with 5 at.% Yb^{3+}, 5 at.% Li^+ and 3 at.% Yb^{3+}, 3 at.% Li^+, as well as the charge for the undoped $ZnWO_4$ crystal. The chemicals were dried at 700 °C before weighting. The weighted amounts of the chemicals were thoroughly mixed and the obtained mixtures were calcined at 700 °C for 5 h to perform a solid phase synthesis of the compound in order to avoid selective evaporation of individual components of the mixture during melting.

We have used WO_3 from two different batches of the same supplier (Lankhit, Ltd., Russia). The batches (labeled as WO_3 #1 and #2) had a supplier-specified purity of 4N and

5N, respectively. ZnO reagent from two suppliers was used. The first one (ZnO #1) was Roanal, Hungary (the purity was not explicitly specified by the supplier). The second source (ZnO #2) was the reagent with a composition of $2ZnCO_3 \times 3Zn(OH)_2 \times H_2O$ (old stock from Krasnyi Khimik, former USSR), with a specified purity of "OSCh 14-2" (4N). This powder was calcined at 900 °C for 10 h before usage. According to the X-ray powder diffraction (XRD) analysis (Siemens D-5000 equipment) and weighting before and after the calcination, the calcined powder contained solely the ZnO phase (within the precision limits of these methods).

The only source of Yb^{3+} ions in our experiments was Yb_2O_3 (YbO-D, Industry Branch Standard 48-206-81, old stock – p/b M-5649, former USSR, purity: 4N). The source of Li^+ ions was Li_2CO_3, again from Krasnyi Khimik with a specified purity of "OSCh 20-2" (4N). $LiCO_3$ was added to the crystal compositions for charge compensation of heterovalent Yb^{3+} entering the Zn^{2+} sub-lattice.

The additional post-growth annealing was performed for color elimination in a vertical cylindrical furnace with Kanthal AF heater. The boules were annealed for 24 h at 800 ºC. The heating and cooling was at a rate of 40 K/h to avoid thermal shocks.

2.2 Crystal characterization

The actual Yb^{3+} concentration N_{Yb} in the crystals was measured by the microprobe analysis using a Cameca Camebax SX-100 analyzer. The impurity composition of the crystals was also analyzed by the spark-source mass-spectrometry (SSMS) using a JEOL JMS-01-BM2 mass-spectrometer.

Differential thermal analysis (DTA) experiment was carried out on a MOM Q-1500 D derivatograph. A Pt-Rh thermocouple and a Pt crucible were used. The heating and cooling rates were 15 °C/min. The sample weight was 350-400 mg. The accuracy for temperature measurement was about ±5 °C.

The structural characterization of the Yb^{3+},Li^+:$ZnWO_4$ crystals was performed by X-ray powder diffraction. The measurements were carried out in a θ - θ Bragg Brentano configuration using a Siemens D-5000 powder X-ray diffractometer with Cu Kα (1.5406 Å) radiation. For structure identification, the XRD pattern was recorded in a 2θ range from 10° to 70°, a step size of 0.02° and a step time of 16 s. For the structure refinement, the XRD pattern was recorded over a broad range of diffraction angles 2θ = 14.5-120° in three subranges: (a) 14.5º to 60º (step size: 0.02º, step time: 16 s), (b) 60º to 92º (step size: 0.02º, step time: 23 s), (c) and 92º to 120º (step size: 0.02º, step time: 32 s). For the Rietveld refinement, the merged diffractogram was converted to counts per second. For temperature dependent (303 - 773 K) XRD studies, we used the same diffractometer with a temperature chamber (HTK10). A heating rate of 0.17 K/s was applied, with a delay of 300 s before each measurement. The 2θ angle varied from 10º to 70º with a step size of 0.03º and a step time of 5 s.

In order to study the coloration of crystals, we measured their unpolarized RT absorption spectra in the wavelength range of 0.3-2.0 μm using a Varian Cary 5000 spectrophotometer.

The Raman spectra were measured with polarized light using a Renishaw inVia Raman microscope with a ×50 objective. The excitation wavelength was 514 nm (Ar^+ laser) and the spectral resolution was ~1 cm^{-1}. The sample for Raman studies was oriented by means of single-crystal XRD.

3. Crystal growth

3.1. Growth of single-crystals

As noted above, the growth direction for the first undoped crystal was spontaneous, whereas the growth direction of all the following samples was lying in the (010) crystallographic plane. A clear trend for natural faceting and cleavage along the (010) plane was observed in all the grown crystals, Fig. 1(a). The faceting and cleavage along other crystallographic planes was less pronounced. The cross-section of the boules had a shape essentially strangulated along the [010] direction, Fig. 1(b,c), as compared to the round one being common for the Cz method. This behavior is assigned to considerably lower thermal conductivity of $ZnWO_4$ along this direction [15].

Using the single-crystalline seeds fabricated from undoped $ZnWO_4$ crystal, first, 5 at.% Yb^{3+}, 5 at.% Li^+: and 3 at.% Yb^{3+}, 3 at.% Li^+:$ZnWO_4$ crystals (nominal compositions) were grown using the available Pt/Rh crucibles. The crystals had a deep black coloration, Fig. 1(a), almost independent of the WO_3 and ZnO batches used. In very thin layers, the crystals were transparent with deep red or brown color. The reasons for this coloration and the ways for its elimination are discussed in Section 3.2. Higher Yb^{3+} content increased the tendency for cracking of the grown crystal boules along the (010) cleavage plane. Note that a crack-free nominally pure (undoped) $ZnWO_4$ crystal has been easily grown using the same procedure.

Later on, we grew several Yb^{3+},Li^+-co-doped crystals using Pt crucibles (without Rh). The shape and the cracking behavior of the crystals was similar to those obtained using the Pt/Rh crucibles. However, the coloration of these samples was different, Fig. 1(d). Even thick (~1 cm) crystal plates were transparent and slightly red-brown colored.

The actual Yb^{3+} doping concentration (in the crystal) N_{Yb} was measured by the microprobe method for the crystal with a nominal composition of 3 at.% Yb^{3+}, 3 at.% Li^+:$ZnWO_4$. It amounted to $2.0\pm0.7\times10^{20}$ cm^{-3} (~1.4 at.% Yb), so that the Yb^{3+} segregation coefficient between the crystal and the melt in the presence of Li^+ charge compensator was evaluated by the equation $K_{Yb} = K_{crystal}/K_{melt}$ to be 0.45 ± 0.16.

The study of the same crystal by the SSMS method yielded the value of 0.54×10^{20} cm^{-3} ($K_{Yb} \geq 0.12$) which is however close to the upper detection limit of the method (about 2000 ppm) and thus it can be considered only as a lower-limit estimate. For the Li^+ ions, the SSMS analysis gave 20 ppm, or, equivalently, $N_{Li} = 0.13\times10^{20}$ cm^{-3} (0.09 at.% Li). Thus, the actual amount of Li^+ is essentially lower than that of Yb^{3+} and charge compensation is in part maintained by other ways, probably, by zinc vacancies.

In Fig. 2, we plotted the dopant segregation coefficients K_D for several TM (Ni, Fe) [32,33] and RE (Yb, Tm, Er, Ho, Dy) [19-21,34-36] ions in $ZnWO_4$. The K_D values show a clear dependence on the dopant ionic radius R_D for VI-fold oxygen coordination [37] (assuming substitution of the Zn^{2+} cations). This dependence is close to $K_D \propto -(R_D - R_{Zn})^2$ in ac-

cordance with well-known Onuma's principle [38]. According to previous studies by inductively coupled plasma atomic emission spectrometry (ICP-AES) performed for a series of RE^{3+}-doped $ZnWO_4$ crystals grown without charge compensators [19,20,34-36], K_{RE} = 0.10-0.30, depending on the cation size and, in particular, K_{Yb} = 0.30 [19]. This value agrees with our observations within the specified error. The residual difference may originate from the use of the Li^+ charge compensator.

Previously, for the isostructural Yb^{3+}:$MgWO_4$ crystal grown by the TSSG method, the Yb^{3+} segregation coefficient between the crystal and the used high-temperature solution K_{Yb} was determined to be 0.13 using ICP-AES [3]. However, in that case, no charge compensators were intentionally added (only some Na^+ cations might have entered from the melt, as Na_2WO_4 was used as a solvent for the crystal growth [5]).

3.2. Crystal coloration

The unpolarized absorption spectra of Yb^{3+},Li^+:$ZnWO_4$ crystals grown using different combinations of ZnO and WO_3 batches in Pt/Rh crucibles are presented in Fig. 3. Here and below, the crystal plates were oriented with their surfaces along the (010) cleavage plane. For all the crystals, absorption related to the $^2F_{7/2} \rightarrow {}^2F_{5/2}$ Yb^{3+} transition is observed at ~1 μm. Besides, intense and broad absorption bands in the visible and near-IR occur. The variation of the ZnO / WO_3 batches leads to a change both in the intensity and position of local maxima of these bands. This effect is more sensitive to the kind of the WO_3 batch. The crystal obtained using the WO_3 (#1) reagent with 4N purity had a super-intense absorption in the visible (at ~500 nm, absorption coefficient α_{abs} >100 cm^{-1}) making it completely black. Besides that, it had an additional band in the near-IR (at ~1.36 μm). The use of the WO_3 (#2) reagent with 5N-purity greatly reduced this absorption yielding a different spectrum. Depending on the ZnO batch, the resolved absorption peaks were at 450 nm (for both batches), at 545 nm (α_{abs} = 25 cm^{-1}, for ZnO #1) or 520 and 600 nm (α_{abs} ~ 18 cm^{-1}, for ZnO #2). Note that the Yb^{3+} band remained unchanged for all the studied crystals.

Uncontrolled impurities. The study of the impurity composition of the grown crystals by SSMS reveals that the main spectroscopically active uncontrolled impurities in all the crystals are the 3d transition-metal (TM) ions of the iron group: Fe, Mn, Ni, Cr and Cu. The content of each of these ions in the crystals exceeded 2 ppm. Their presence is facilitated by the fact that $FeWO_4$, $MnWO_4$, $NiWO_4$, *etc*., crystallize with the same structure as $ZnWO_4$ and form isostructural series with it. In particular, the crystal grown using WO_3 #1 contained a lot of Fe (200 ppm) and Ni (20 ppm), see Table 1, as compared to crystals grown with WO_3 #2. On the contrary, the use of the WO_3 #2 reagent led to a higher content of Cu (20 ppm). The concentrations of Cr and Mn were comparable in both cases, ~6-10 ppm. One should also note the essential amount of Rh in both crystals, 40-80 ppm. Obviously, the used Pt/Rh crucible is the source of this impurity.

Annealing. Relatively thick (thickness t = 3.6 mm) crystalline plates cut from the 5 at.% Yb^{3+}, 5 at.% Li^+:$ZnWO_4$ crystal (nominal composition) grown from the Pt/Rh crucible using WO_3 #2 and ZnO #1 were annealed in air at 800 °C for 3 weeks. After annealing, the crystalline plates changed their coloration from black to brownish-red, as shown at the inset of

Fig. 4(a). The comparison of the absorption spectra before and after annealing, Fig. 4(a), indicates that the intensity of the broad absorption band in the visible (centered at ~545 nm) is drastically reduced after this treatment. The calculated differential absorption spectrum ($\Delta\alpha_{abs} = \alpha_{as\text{-}grown} - \alpha_{annealed}$) is similar to that of black-colored scheelite-like double molybdate crystals grown in oxygen-deficient atmospheres [39-41]. It contains an intense band spanning from 0.5 to 1 μm and centered at ~580 nm ($\Delta\alpha_{abs}$ = 21 cm^{-1}). In [39-41], a similar absorption band was assigned to F-centers (free electrons localized at oxygen vacancies). After annealing, the absorption spectrum contains two distinct peaks at ~440 and ~530 nm (α_{abs} ~8-9 cm^{-1}).

For comparison, we also studied an undoped $ZnWO_4$ crystal grown in a Pt/Rh crucible with the use of WO_3 #2 and ZnO #2 reagents. The absorption spectra of the crystal plate (t = 0.7 mm) before and after the annealing at 800 °C for 3 weeks (the same regime as applied above), see Fig. 4(b), were similar to those shown in Fig. 4(a) except for the lack of Yb^{3+} absorption at ~1 μm. The intensity of the bands at ~430 and 520 nm was redistributed and their peak wavelengths slightly shifted. This indicates a possible indirect effect of Yb^{3+} ions on the nature of these optical centers, probably via the alteration of the local multi-ligands.

In Fig. 4(c), we compare two samples of different thickness (t = 0.9 mm and 3.6 mm) cut from the same sample grown using the ZnO (#1) and WO_3 (#2) reagents. Accordingly, different duration of the oxidizing annealing was needed: 24 h and 3 weeks, respectively. After this time, no noticeable change in the absorption spectrum was detected. The spectra are very similar and the peak absorption at ~520-530 nm (α_{abs} ~8 cm^{-1}) is nearly the same.

Crucible composition. Finally, we studied the influence of the crucible composition on the crystal coloration. We grew a 5 at.% Yb^{3+}, 5 at.% Li^+:$ZnWO_4$ crystal (nominal composition) from a rhodium free Pt crucible with the use of the WO_3 #2 and ZnO #1 batches. Unlike all the previous samples grown from the Pt/Rh crucible, this crystal appeared to be transparent with only light pink-brown coloration (even without oxidizing annealing), Fig. 1(d). A similar coloration of undoped $ZnWO_4$ is presented in [42]. The absorption spectrum of the as-grown crystal is shown in Fig. 5. In the spectrum, a weak and broad band centered at ~450 nm (α_{abs} ~1.8 cm^{-1}) is present.

For the Yb^{3+},Li^+:$ZnWO_4$ crystals grown using the Pt/Rh crucibles, the UV absorption edge λ_{UV} is at ~380 nm (after the oxidizing annealing). For the crystals grown from a Pt crucible, it is shorter, λ_{UV} ~340 nm, corresponding to an optical bandgap of 3.65 eV. The electronic structure of $ZnWO_4$ was studied in [43] revealing that it is a direct bandgap material with the minimum of the conduction band and the maximum of the valence band at the same Y point of the Brillouin zone (calculated E_g ~4.65 eV). Experimental optical studies of undoped $ZnWO_4$ gave the E_g value of 3.9-4.4 eV [44]. Thus, the observed difference in the position of the UV absorption edge may be associated with some local optical centers (see Section 3.3).

3.3. Discussion

The coloration of Yb^{3+}-doped $ZnWO_4$ crystals is a relevant issue because it may affect their laser performance. Let us discuss existing literature on the topic (mostly, for nominally pure (undoped) $ZnWO_4$ crystals) and interpret the findings of the present work.

The growth of *undoped* $ZnWO_4$ crystals by the Cz method is known for many years. One of the first reports devoted to this crystal is the paper by O'Hara [45]. It was revealed that the use of Rh crucibles (unlike Pt ones) gave rise to black melts and opaque crystals. However, neither absorption spectra, nor any discussion about the reasons of black coloration nor attempts to eliminate it by oxidizing annealing are given in this paper. Nagornaya *et al.* reported on the Cz growth of large and transparent $ZnWO_4$ crystals from Pt crucibles [25]. The authors annealed the as-grown boules at 800-1000 °C in oxygen leading to a change of the crystal coloration from brownish to slightly pink-violet without giving details. Galashov *et al.* reported on further improvement of the quality of undoped $ZnWO_4$ crystals [26]. The authors used for the growth performed in Pt crucibles high-purity reagents (a home-made WO_3 and commercial ZnO with concentration of impurity TM ions down to 1 ppm). In [26], the transmission spectra of $ZnWO_4$ before and after annealing were presented without giving many details. Despite the excellent purity of the starting growth charge, the as-grown crystals exhibited weak absorption at ~500 nm (α_{abs} ~ 0.10 cm^{-1}). The discussion about the nature of residual coloration is absent in this paper. A systematic study of the optical absorption of $ZnWO_4$ crystals with various coloration was performed by Limarenko *et al.* [28]: from almost colorless to pink, dark pink and yellow. The authors discussed such aspects as the possible assignment of the observed absorption bands to different optical active centers (mainly, iron ions), the influence of the crystal annealing in different atmospheres on its residual coloration and the effect of various decolorating agents (Sb, Bi, Ag, *etc*.) onto such a coloration.

There also exist studies of $ZnWO_4$ in which the colorating and decolorating impacts of various impurities were studied by *a deliberate doping* of the crystal by such impurities. One clear example is iron doping. The segregation coefficient of iron (Fe) in $ZnWO_4$ is close to unity [33] and, as a result, it is easily introduced in the crystal in its both valent forms (Fe^{2+} and Fe^{3+}). $FeWO_4$ crystallizes with the same structure as zinc oxide and forms a solid solution with it. Both ions substitute for the Zn^{2+} ones in the lattice. Földvári *et al.* studied Fe-doped $ZnWO_4$ crystals [46]. The absorption at ~460 and 350 nm was assigned to Fe^{2+} and Fe^{3+} species, respectively. Watterich *et al.* have also assigned the absorption of $ZnWO_4$ crystals at ~460 nm to the divalent iron, Fe^{2+} [27,33]. Therefore, one of the absorption peaks revealed in our crystals (around 430-440 nm) can be assigned to Fe^{2+} impurity. Bencs *et al.* discussed the possible ways to remove the coloration of $ZnWO_4$ induced by Fe^{2+} and Cr^{3+} impurity ions, i.e., by (i) applying an electric field during growth, (ii) using a subsequent oxidizing treatment, (iii) adding decoloration agents (e.g., Sb^{5+}) to the melt or (iv) using chemical purification of the starting materials [47]. Kornylo *et al.* investigated Fe,Li-co-doped $ZnWO_4$ [48]. This study reported on a reduction in the crystal coloration owing to the Li^+ codoping, as highlighted by the decrease of the absorption at ~460 nm due to the $Fe^{2+} \rightarrow Fe^{3+}$ transformation. The same effect was also assumed in [27]. Therefore, it can be suggested that in our case, besides acting as a charge compensator, the addition of Li^+ into the ZnWO4 crystals may be in part responsible for the reduced absorption at 430-440 nm. Another impurity ion,

which was proposed as a source of $ZnWO_4$ coloration is trivalent chromium. In particular, Cr^{3+} was considered as the main source of pinkish coloration of undoped $ZnWO_4$ crystals in [27].

The *point defects* in $ZnWO_4$ and their effect on the crystal coloration have also been studied. In particular, in the papers [27,33], the crystals still presented slight pink coloration with an optical absorption at ~510 nm after removing Fe^{2+}. Oxygen vacancies, OH^- groups, or W^{5+} ions were proposed as possible sources of this absorption in [33] although they were ruled out in [27]. As a result, Cr^{3+} was suggested as the possible source of pinkish coloration of undoped crystals. The electron spin resonance studies of $ZnWO_4$ crystals revealed impurity centers with small concentrations (few ppm) such as Cr^{3+}, Mn^{2+}, Fe^{3+}, Co^{2+}, Cu^{2+}, Rh^{2+} and Pt^{3+} [33]. The latter two ions may enter into the crystal from the crucible material (Pt or Rh), while the TM ions are associated with the growth charge as impurities from the reagents. In the presence of Li^+ as a charge compensator, as mentioned above, divalent iron is suppressed at the expense of raising the amount of Fe^{3+}, and, moreover, Cr^{3+} impurity ions may be promoted to enter the lattice. Thus, the pink coloration of Li^+-doped $ZnWO_4$ was assigned in [27,28] to Cr^{3+}. Wang *et al.* reported on the growth of both clear and colored $ZnWO_4$ crystals [49]. In the latter case, two bands in the excitation spectra centered at ~496 and 520 nm were observed. The corresponding emission was assigned to defects. It was pointed out that annealing of the colored crystals in oxygen atmosphere can remove their coloration, as expressed by the disappearance of the absorption in the visible.

Thus, the problem of coloration of undoped $ZnWO_4$ crystals is well-known and it can be eliminated to a great extent by (i) using specially purified WO_3 and ZnO reagents, (ii) applying annealing in oxygen atmosphere and (iii) introducing decolorating agents. However, the influence of the crucible composition (in particular, the role of Rh) has been barely studied. Moreover, such analysis has never been performed for Yb^{3+}-doped crystals.

The information about the coloration and defects of RE-doped $ZnWO_4$ crystals is scarce. There is a series of studies dedicated to the growth and characterization of $ZnWO_4$ crystals with various RE^{3+} dopants (RE = Yb, Er, Tm, Ho, Dy) [19,20,34-36], however, without giving details about their coloration. Nevertheless, in the absorption spectra of Ho^{3+}:$ZnWO_4$ given in [36], a strong absorption band in the visible, at ~500 nm (α_{abs} ~5 cm^{-1}) is shown. Kowalski *et al.* reported on the growth of undoped, Ca^{2+}-doped and Ca^{2+},Eu^{3+}-co-doped $ZnWO_4$ crystals [50]. Particularly in the latter case, a dark internal part of the grown boule was detected indicating the effect of the RE^{3+} ions.

Taking into account the literature data and our results, we can assume that for the as-grown crystals obtained using relatively pure reagents (e.g., ZnO #1 and WO_3 #2) and Pt/Rh crucibles, there are probably two main sources of absorption in the visible, namely (i) the iron ions (the band from Fe^{3+} at ~350 nm, manifested by the red-shift of the UV absorption edge, and the band from Fe^{2+} at ~450 nm) and (ii) the F-centers based on free electrons localized at oxygen vacancies (the broad band centered at ~580 nm spanning into the near-IR). The latter defects result from a partial reduction of the crystal composition that leads to losing a part of oxygen. Moreover, it is obvious that rhodium from the crucible acts as a catalyst for such a reduction. Rhodium (like all other metals of platinum group) is well-known to have a strong

catalytic activity in respect to many redox chemical reactions, which is widely used in chemical industry. Note that in [51], the coloration of oxide crystals with oxygen vacancies was assigned to small polarons rather than F-centers while there is no evidence of such assignment for tungstate crystals.

A combination of the above mentioned optical centers leads to black coloration of the as-grown crystals. The oxidizing annealing removes the oxygen vacancies and reduces the amount of the Fe^{2+} species simultaneously giving rise to the Fe^{3+} ones. As a result, the annealed crystalline samples are pinkish. This color is determined by the residual Fe^{2+} species (the band at ~440-450 nm) and by the band at ~520-530 nm the nature of which is still unknown. This band cannot be assigned to Cr^{3+} (see [27,28]) due to the following reasons: (i) the absorption spectra of $ZnWO_4$ crystals intentionally doped by chromium revealed two almost equal in intensity absorption bands at ~520 and 700 nm and the latter one is not observed in our case, and (ii) the absorption cross-section obtained by dividing the peak absorption coefficient at ~520 nm by the actual Cr^{3+} concentration in our crystals (see Section 3.2) is by order of magnitude higher than the values commonly accepted for parity forbidden $^4A_2 \rightarrow {}^4T_1$ vibronic transition of Cr^{3+}. In addition, it seems that the use of the Pt crucibles (instead of the Pt/Rh ones) somehow diminishes the concentration of TM ion-related defects (for the same composition of the growth charge).

4. Crystal structure

4.1. Differential thermal analysis

The DTA curves for the 5 at.% Yb^{3+}, 5 at.% Li^+:$ZnWO_4$ crystal (nominal composition) corresponding to sample heating and cooling are shown in Fig. 6. One can see just one strong and reversible endothermic (at heating) and exothermic (at cooling) effect, which, certainly, corresponds to the congruent melting of the compound. The starting temperature of melting and that of crystallization well correspond to each other at 1166 ºC, in contrast to the DTA curve for undoped $ZnWO_4$ given in [42], where these two temperatures differed by more than 30 ºC. The determined melting point for 5 at.% Yb^{3+}, 5 at.% Li^+:$ZnWO_4$ is by 22 °C lower as compared with the data given for the undoped crystal [23]. Lowering of the melting point of a crystal with introduction of impurities into its composition is a usual situation. The absence of any additional thermal effects reflects the absence of polymorphic phase transformations of the 1st type below the melting point.

4.2. Structure refinement

The crystal structure and the phase purity of the crystals were confirmed using XRD. The RT XRD pattern of the 5 at.% Yb^{3+}, 5 at.% Li^+:$ZnWO_4$ crystal (nominal composition) is shown in Fig. 7. The crystal composition of $Zn_{0.964}Yb_{0.018}Li_{0.018}WO_4$ was assumed. The actual concentration of Yb (1.8 at.%) was determined by the micro-probe analysis and an equal atomic fraction of Yb and Li was considered. The relative intensity and position of the diffraction peaks of the sample agree well with the JCPDS (Joint Committee on Powder Diffraction Standards) card #96-210-1676 for undoped $ZnWO_4$. No other phases except the monoclinic one are found. All this indicates that the sample is of single-phase nature. The XRD

pattern measured for a broader range of diffraction angles 2θ of 14.5-120° was refined by the Rietveld method using the FULLPROF package; the calculated pattern showed a good matching with the experimental one, Fig. 8. The crystal structure of undoped $ZnWO_4$ [52] was taken as the starting model for the Rietveld refinement.

Yb^{3+},Li^+:$ZnWO_4$ is monoclinic belonging to the space group $P2/c$ – C^4_{2h}, No. 13 and the centrosymmetric point group $2/m$. The lattice constants are a = 4.702(2) Å, b = 5.718(6) Å, c = 4.930(4) Å, the unit cell volume V_{calc} = 132.571 Å^3, the monoclinic angle $\beta = \boldsymbol{a}\hat{}\boldsymbol{c}$ = 90.713(5)° and the theoretical crystal density ρ_{calc} = 7.553 g/cm^3 (the number of the formula units Z = 2). The R-factors were R_{wp} = 11.6 and R_p = 8.11 (the reduced chi-squared value $\chi^2 = (R_{wp}/R_{exp})^2$ = 7.03 and the Bragg factor R_b = 0.89), cf. Table 2. The obtained fractional atomic coordinates are listed in Table 3.

The determined lattice constants are slightly higher than those for an undoped $ZnWO_4$ crystal (a = 4.69263(5) Å, b = 5.72129(7) Å, c = 4.92805(5) Å and β = 90.6321(9)°) [7], see also Table 4. The higher precision in the reported lattice constants for undoped $ZnWO_4$ is explained by the use of neutron diffraction in [7].

The Yb^{3+} ions in $ZnWO_4$ are expected to replace the Zn^{2+} cations. The charge compensation is partially maintained by Li^+ cations and the excessive charge difference originating from the remaining Yb^{3+} ions is most likely compensated by cationic (probably, zinc) vacancies (see Section 3.1). There is a single crystallographic site for Zn^{2+} in the structure of $ZnWO_4$ (Wyckoff symbol: 2*e*, symmetry: C_2). The Zn^{2+} cations are located in the [ZnO_6] octahedra and, consequently, they are VI-fold oxygen-coordinated. The ionic radii of the cations involved in the doping process are 0.868 Å (Yb^{3+}), 0.74 Å (Zn^{2+}) and 0.76 Å (Li^+) [37], so that an increase of the unit-cell volume is expected. The significant difference of the ionic radii of Zn^{2+}, Yb^{3+} and Li^+, as well as the difference of their valence are expected to result in inhomogeneous broadening of the absorption and luminescence spectral bands of Yb^{3+} ions.

The structure of Yb^{3+},Li^+-doped $ZnWO_4$ is shown in Fig. 9 according to the atomic coordinates determined by the Rietveld refinement. The metal – oxygen (M – O) interatomic distances in the [WO_6] and [(Zn|Yb|Li)O_6] polyhedra determined by the analysis of the cif file by VESTA software are listed in Table 5. W^{6+} is bonded to six oxygen ions O^{2-} forming distorted [WO_6] octahedra that share corners with eight equivalent [(Zn|Yb|Li)O_6] octahedra, and edges with two equivalent [WO_6] octahedra as shown in projection on the crystallographic plane ***b*-*c***. The W – O bond lengths are in the range 1.752(2) – 2.166(4) Å, see Fig. 10(a). Zn^{2+}|Yb^{3+}|Li^+ is bonded to six oxygen cations O^{2-} to form [(Zn|Yb|Li)O_6] octahedra which, in their turn, share corners with eight equivalent [WO_6] octahedra and edges with two equivalent [(Zn|Yb|Li)O_6] ones. There are two shorter (1.981(0) Å), two intermediate (2.032(9) Å) and two longer (2.319(5) Å) Zn–O bond lengths, Fig. 10(b).

As a result, the structure of Yb^{3+},Li^+:$ZnWO_4$ is a chain structure determined by zig-zag chains formed by edge-sharing [(Zn|Yb|Li)O_6] octahedra or edge-sharing [WO_6] octahedra running parallel to the ***c***-axis. Each chain formed by [(Zn|Yb|Li)O_6] is corner-linked to four chains formed by [WO_6]. Thus, the structure contains open channels also going parallel to the ***c***-axis. The shortest distance Zn|Yb–Zn|Yb observed in Yb^{3+},Li^+:$ZnWO_4$ is 3.269(6) Å along the vector [u v w] = [0 -0.3756 0.5].

Besides, it is clear from Fig. 9(b) that the structure of $ZnWO_4$ contains [WO_6] layers bonded to each other by Zn^{2+} ions only. These ions are not very strong bonders and the breaking energy of the [O-Zn-O] chemical bond (which is predominantly ionic) is not very high. Therefore, the existence of very well expressed cleavage plane in this crystal is easily explainable. Moreover, when the crystal is doped with Yb^{3+} ions with not enough amount of the charge compensator (that is somehow valid in our case), a substantial concentration of zinc vacancies may appear. It should additionally weaken the bonds between the neighboring [WO_6] layers in the crystal structure leading to enhanced cleavage ability. This phenomenon occurred in the Yb^{3+},Li^{+}-co-doped $ZnWO_4$ crystals grown in the present work. An increase of the crystal cracking was observed previously for $CdWO_4$ crystals [42] which are isostructural to $ZnWO_4$ in the case of Cd^{2+} deficiency. Thus, optimization of charge compensation during the crystal growth will probably help to reduce the cracking of Yb^{3+}-doped $ZnWO_4$ crystals in further studies.

4.3. Thermal expansion

The unit-cell parameters as a function of temperature T were refined with the FULLPROF program. The relative evolution of the parameters $L = a$, b, c and $c^* = c\times\cos(\beta - 90^o)$ with respect to their values at 303 K (L_{303K}), Fig. 11, was used to determine the components of the linear thermal expansion tensor, $\alpha = (\Delta L/L_{303K})/\Delta T$, in the crystallophysical frame with the mutually orthogonal axes (i.e., $X_1 \parallel \boldsymbol{a}$, $X_2 \parallel \boldsymbol{b}$ and $X_3 \parallel \boldsymbol{c^*}$). All the unit-cell parameters increase nearly linearly with temperature indicating a positive thermal expansion. The monoclinic angle β slightly increases with T.

The linear thermal expansion tensor in the crystallophysical frame is:

$$\alpha_{ij} = \begin{pmatrix} 11.710 & 0 & -0.006 \\ 0 & 9.901 & 0 \\ -0.006 & 0 & 7.009 \end{pmatrix} \times 10^{-6}\,\mathrm{K}^{-1}.$$

The non-diagonal $\alpha_{13} = \alpha_{31}$ elements are very small and the tensor is quasi-diagonal. The eigen-frame of this tensor in which it takes the diagonal form is very close to the crystallophysical one, $X'_1 \parallel \boldsymbol{a}$, $X'_2 \parallel \boldsymbol{b}$ and $X'_3 \parallel \boldsymbol{c^*}$, see Fig. 12.

The eigen-values of the thermal expansion tensor of Yb^{3+},Li^{+}:$ZnWO_4$ are $\alpha'_{11} \approx \alpha_a = 11.71\times10^{-6}$ K^{-1}, $\alpha'_{22} = \alpha_b = 9.90\times10^{-6}$ K^{-1} and $\alpha'_{33} \approx \alpha_{c^*} = 7.01\times10^{-6}$ K^{-1}. Thus, the anisotropy of the thermal expansion is relatively weak, as expressed by the ratios $\alpha'_{11} : \alpha'_{33} = 1.67$ and $\alpha'_{22} : \alpha'_{33} = 1.41$. The coefficient of the volumetric thermal expansion $\alpha_{vol} = \alpha'_{11} + \alpha'_{22} + \alpha'_{33} = 28.62\times10^{-6}$ K^{-1}.

In Table 6, we compare the thermal expansion coefficients for various $M^{2+}WO_4$ crystals reported so far [4,5,14,53]. Our results are close to previously reported values for a Ho^{3+}:$MgWO_4$ crystal, $\alpha_a = 11.22\times10^{-6}$ K^{-1}, $\alpha_b = 8.09\times10^{-6}$ K^{-1} and $\alpha_c = 8.77\times10^{-6}$ K^{-1} [5].

5. Raman spectra

The polarized RT Raman spectra of the 5 at.% Yb^{3+}, 5 at.% Li^{+}:$ZnWO_4$ crystal (nominal composition) are shown in Fig. 13. The measurements were carried out using a rectangular sample cut in the crystallophysical frame {$\boldsymbol{a}$, $\boldsymbol{b}$, $\boldsymbol{c^*}$}. For simplicity, we will designate $\boldsymbol{c^*}$

as ***c*** due to the closeness of the monoclinic angle to the right angle, within the accuracy of the sample orientation. The Porto's notations for Raman spectroscopy, $m(nk)\bar{l}$, are used, where m and l are the directions of propagation of the incident and scattered light, and n and k are the corresponding polarization states [54]. We studied all three principal crystal cuts: ***a***-cut, ***b***-cut and ***c***-cut.

The primitive cell of $ZnWO_4$ contains two formula units (Z = 2). The factor group analysis predicts a total of 36 degrees of freedom for 12 atoms in each primitive cell. The corresponding irreducible representations at the center of the Brillouin zone Γ (***k*** = 0) are $8A_g + 10B_g + 8A_u + 10B_u$ of which the even (*gerade*, *g*) vibrations are Raman-active and the others are IR-active [55]. Thus, 18 Raman modes ($8A_g + 10B_g$) are possible. We observed 17 modes out of 18 possible ones (except for the low-frequency one at <100 cm^{-1}). The modes are labeled in Fig. 13 and their peak frequencies and symmetries (A_g or B_g) are listed in Table 7. Here, the assignment is according to [56,57].

Monotungstates are well-known Raman-active materials. One prominent example is $CaWO_4$, having a tetragonal (scheelite-type) structure (sp. gr. $I4_1/a$). For this material, the Raman spectra can be divided into two sets of frequencies at 0-409 cm^{-1} and 797-912 cm^{-1}, showing a characteristic "gap" at intermediate frequencies. This "gap" is related to tightly bound atoms in the $[WO_4]^{2-}$ molecular group with internal vibrations generally occurring at higher frequencies. In contrast, the external vibrations due to the loosely bound Ca^{2+} and $[WO_4]^{2-}$ occur at lower frequencies. Such a behavior is not observed in $ZnWO_4$ due to the closeness of two tungstate groups $[WO_4]$ corresponding to the octahedra $[WO_6]$. It is only possible to attribute the high-frequency modes at 707 cm^{-1} (A_g) and 785 cm^{-1} (B_g) (both assigned as v_2) and at 906 cm^{-1} (A_g) (assigned as v_1) to internal (stretching) vibrations of the W – O atoms in the $[WO_6]$ octahedra [55,56].

The Raman spectra are strongly polarized. The most intense band in the spectra is found at 906.0 cm^{-1}. Its full width at half maximum (FWHM) Δv is 11.9 cm^{-1}. This band is slightly shifted and broadened as compared to undoped $ZnWO_4$ for which v_1 = 906.8 cm^{-1} and the corresponding Δv = 8.3 cm^{-1} (all the values specified at RT) [56]. Yb^{3+},Li^+:$ZnWO_4$ is a high phonon energy material.

The Yb^{3+},Li^+:$ZnWO_4$ crystals are promising for self-Raman conversion of the fundamental radiation (~1.05 μm, the $^2F_{5/2} \rightarrow {}^2F_{7/2}$ Yb^{3+} transition) to the spectral range of ~1.16 μm. Kaminski *et al.* demonstrated Stokes and anti-Stokes stimulated Raman scattering relying on the ~906 cm^{-1} mode in undoped $ZnWO_4$ using pulses with picosecond duration [57].

6. Conclusions

To conclude, we have grown for the first time Yb^{3+},Li^+-co-doped $ZnWO_4$ crystals with the goal of developing a novel laser gain material at ~1 μm. This compound melts congruently at 1166 ºC and large-volume crystals were obtained by the conventional Czochralski method. Yb^{3+},Li^+:$ZnWO_4$ crystallizes in the monoclinic system (sp. gr. $P2/c$). The main issues for fabrication of laser-quality crystals are (i) suppressing the unwanted crystal coloration; (ii) avoiding excessive crystal cracking which seems to be enhanced by Yb^{3+} doping despite the

relatively weak anisotropy of thermal expansion; and (iii) reaching high actual Yb^{3+} doping concentrations for efficient optical pumping.

We studied in detail the coloration of as-grown Yb^{3+},Li^{+}:$ZnWO_4$ crystals as a function of the purity of the reagents (WO_3 and ZnO) and crucible composition (Pt/Rh and Pt). For crystals grown from the Pt/Rh crucibles, the coloration caused mainly by the oxygen vacancies can be greatly eliminated by oxidizing annealing at ~800 °C for 1 – 20 days (depending on the sample thickness). The nature of the residual pink coloration of samples is probably due to iron ions, as well as other uncontrolled impurities. Therefore, it can be further eliminated by special purification of the growth charge. The material of the crucible seems to affect the coloration of the crystals acting as a catalyst of a partial reduction of the crystal-forming compound and promoting formation of other impurity centers, such as Fe^{2+}(Fe^{3+}), *etc*. in the case of Rh. Thus, there exist two possibilities for obtaining laser-quality Yb^{3+},Li^{+}:$ZnWO_4$: (i) the use of Pt/Rh crucibles and a subsequent oxidizing annealing, or (ii) the use of pure Pt crucibles.

Our studies indicate a moderatelly high segregation coefficient for Yb^{3+} ions in $ZnWO_4$ (K_{Yb} = 0.45±0.16), despite the heterovalent doping mechanism and the notable difference of ionic radii of Yb^{3+} and Zn^{2+}. Indeed, K_{Yb} well exceeds that for the isostructural $MgWO_4$ crystal. This is assigned in part to the used charge compensator (Li^{+}). Further studies are needed to clarify the role of oxygen vacancies and Li^{+} cations in the doping mechanism of $ZnWO_4$. An optimization of the Li^{+} content in the charge, and / or the search of a more appropriate charge compensator should be performed.

The quality of obtained crystals was sufficient to achieve diode-pumped laser operation with Yb^{3+},Li^{+}:$ZnWO_4$ at ~1 μm (see the parallel paper [29]).

Acknowledgements

This work was supported by the Spanish Government (project No. MAT2016-75716-C2-1-R (AEI/FEDER,UE)) and by Generalitat de Catalunya (project No. 2017SGR755). The research work of the authors from Prokhorov General Physics Institute was supported by Russian Scientific Fund (grant # 18-12-00517.)

References

1. E. Cavalli, A. Belletti, M. G. Brik, Optical spectra and energy levels of the Cr^{3+} ions in MWO_4 (M = Mg, Zn, Cd) and $MgMoO_4$ crystals, J. Phys. Chem. Solids 69 (2008) 29-34.

2. L. Li, Y. Yu, G. Wang, L. Zhang, Z. Lin, Crystal growth, spectral properties and crystal field analysis of Cr^{3+}:$MgWO_4$, Cryst. Eng. Comm. 15 (2013) 6083-6089.

3. L. Zhang, W. Chen, J. Lu, H. Lin, L. Li, G. Wang, G. Zhang, Z. Lin, Characterization of growth, optical properties, and laser performance of monoclinic Yb:$MgWO_4$ crystal, Opt. Mater. Express 6 (2016) 1627-1634.

4. X. Wang, Z. Fan, H. Yu, H. Zhang, J. Wang, Characterization of $ZnWO_4$ Raman crystal, Opt. Mater. Express 7 (2017) 1732-1744.

5. L. Zhang, P. Loiko, J. M. Serres, E. Kifle, H. Lin, G. Zhang, E. Vilejshikova, E. Dunina, A. Kornienko, L. Fomicheva, U. Griebner, V. Petrov, Z. Lin, W. Chen, K. Subbotin, M. Aguiló, F.

Díaz, X. Mateos, Growth, spectroscopy and first laser operation of monoclinic Ho^{3+}:$MgWO_4$ crystal, J. Lumin. 213 (2019) 316-325.
6. V. B. Kravchenko, Crystal structure of the monoclinic form of magnesium tungstate $MgWO_4$, J. Struct. Chem. 10 (1969) 139-140.
7. P. F. Schofield, K. S. Knight, G. Cressey, Neutron powder diffraction study of the scintillator material $ZnWO_4$, J. Mater. Sci. 31 (1996) 2873-2877.
8. V. B. Mikhailik, H. Kraus, V. Kapustyanyk, M. Panasyuk, P. Yu, V. Tsybulskyi, L. Vasylechko, Structure, luminescence and scintillation properties of the $MgWO_4$–$MgMoO_4$ system, J. Phys.: Cond. Matter 20 (2008) 365219.
9. F. A. Danevich, D. M. Chernyak, A. M. Dubovik, B. V. Grinyov, S. Henry, H. Kraus, V. M. Kudovbenko, V. B. Mikhailik, L. L. Nagornaya, R. B. Podviyanuk, O. G. Polischuk, I. A. Tupitsyna, Y. Y. Vostretsov, $MgWO_4$ – A new crystal scintillator, Nucl. Instrum. Meth. A 608 (2009) 107-115.
10. T. Oi, K. Takagi, T. Fukazawa, Scintillation study of $ZnWO_4$ single crystals, Appl. Phys. Lett. 36 (1980) 278-279.
11. L. L. Nagornaya, B. V. Grinyov, A. M. Dubovik, Y. Y. Vostretsov, I. A. Tupitsyna, F. A. Danevich, V. M. Mokina, S. S. Nagorny, O. G. Shkulkova, H. Kraus, V. B. Mikhailik, Large volume $ZnWO_4$ crystal scintillators with excellent energy resolution and low background, IEEE Trans. Nucl. Sci. 56 (2009) 994-997.
12. H. Kraus, V. B. Mikhailik, Y. Ramachers, D. Day, K.B. Hutton, J. Telfer, Feasibility study of a $ZnWO_4$ scintillator for exploiting materials signature in cryogenic WIMP dark matter searches, Phys. Lett. B 610 (2005) 37-44.
13. P. Belli, R. Bernabei, F. Cappella, R. Cerulli, C.J. Dai, F.A. Danevich, B. V. Grinyov, A. Incicchitti, V. V. Kobychev, L. L. Nagornaya, S. S. Nagorny, Search for 2β processes in ^{64}Zn with the help of $ZnWO_4$ crystal scintillator, Phys. Lett. B 658 (2008) 193-197.
14. L. Zhang, Y. Huang, S. Sun, F. Yuan, Z. Lin, G. Wang, Thermal and spectral characterization of Cr^{3+}:$MgWO_4$ – a promising tunable laser material, J. Lumin. 169, Part A (2016) 161-164.
15. P. A. Popov, S. A. Skrobov, A. V. Matovnikov, N. V. Mitroshenkov, Y. A. Borovlev, Thermal conductivity and heat capacity of a $ZnWO_4$ crystal, Phys. Solid State 58 (2016) 853-856 [transl. from Fizika Tverdogo Tela 58 (2016) 827–830)].
16. P. Loiko, M. Chen, J. M. Serres, M. Aguiló, F. Díaz, H. Lin, G. Zhang, L. Zhang, Z. Lin, P. Camy, S.-B. Dai, Z. Chen, Y. Zhao, L. Wang, W. Chen, U. Griebner, V. Petrov, X. Mateos, Spectroscopy and high-power laser operation of a monoclinic Yb^{3+}:$MgWO_4$ crystal, Opt. Lett. 45 (2020) 1770-1773.
17. P. Loiko, J. M. Serres, X. Mateos, M. Aguiló, F. Díaz, L. Zhang, Z. Lin, H. Lin, G. Zhang, K. Yumashev, V. Petrov, U. Griebner, Y. Wang, S. Y. Choi, F. Rotermund, W. Chen, Monoclinic Tm^{3+}:$MgWO_4$: a promising crystal for continuous-wave and passively Q-switched lasers at ~2 μm, Opt. Lett. 42 (2017) 1177-1180.
18. Y. Wang, W. Chen, M. Mero, L. Zhang, H. Lin, Z. Lin, G. Zhang, F. Rotermund, Y. J. Cho, P. Loiko, X. Mateos, U. Griebner, V. Petrov, Sub-100 fs Tm:$MgWO_4$ laser at 2017 nm mode locked by a graphene saturable absorber, Opt. Lett. 42 (2017) 3076-3079.
19. F. Yang, The spectroscopic investigation of $ZnWO_4$:Yb^{3+} single crystal, J. Mater. Res. 27 (2012) 2096-2100.

20. F. Yang, C. Tu, The spectroscopy investigation of $ZnWO_4$:Tm^{3+} single crystal, J. Alloys Compd. 535 (2012) 83-86.
21. Z. Xia, F. Yang, L. Qiao, F. Yan, End pumped yellow laser performance of Dy^{3+}:$ZnWO_4$, Opt. Commun. 387 (2017) 357-360.
22. P. Loiko, L. Zhang, J.M. Serres, Y. Wang, M. Aguiló, F. Díaz, Z. Lin, H. Lin, G. Zhang, E. Vilejshikova, E. Dunina, A. Kornienko, L. Fomicheva, V. Petrov, U. Griebner, W. Chen, X. Mateos, Monoclinic Tm^{3+}:$MgWO_4$ crystal: Crystal-field analysis, tunable and vibronic laser demonstration, J. Alloys Compd. 763 (2018) 581-591.
23. D. M. Trots, A. Senyshyn, L. Vasylechko, R. Niewa, T. Vad, V. B. Mikhailik, H. Kraus, Crystal structure of $ZnWO_4$ scintillator material in the range of 3–1423 K, J. Phys.: Cond. Matter 21 (2009) 325402.
24. S. O'hara, G.M. McManus, Czochralski growth of low-dislocation-density zinc tungstate crystals, J. Appl. Phys. 36 (1965) 1741-1746.
25. L. L. Nagornaya, A. M. Dubovik, Y. Y. Vostretsov, B. V. Grinyov, F. A. Danevich, K. A. Katrunov, V. M. Mokina, G. M. Onishchenko, D. V. Poda, N. G. Starzhinskiy, I. A. Tupitsyna, Growth of $ZnWO_4$ crystal scintillators for high sensitivity 2β experiments, IEEE Trans. Nucl. Sci. 55 (2008) 1469-1472.
26. E. N. Galashov, V. A. Gusev, V. N. Shlegel, Y. V. Vasiliev, The growth of $ZnWO_4$ and $CdWO_4$ single crystals from melt by the low thermal gradient Czochralski technique," Cryst. Rep. 54 (2009) 689-691 [transl. from Kristallografiya 54 (2009) 733–735].
27. A. Watterich, O. R. Gilliam, L. A. Kappers, Colouration, impurities and non-local charge-compensation in $ZnWO_4$, Solid State Commun. 88 (1993) 619-621.
28. L. N. Limarenko, Y. V. Zorenko, M. M. Batenchuk, Z. T. Moroz, M. V. Pashkovskii, I. V. Konstankevich, Role of intrinsic defects and impurities in forming the optical characteristics of $ZnWO_4$ and $CdWO_4$ crystals, J. Appl. Spectr. 67 (2000) 287-294.
29. A. Volokitina, S.P. David, P. Loiko, K. Subbotin, A. Titov, D. Lis, R.M. Solé, V. Jambunathan, A. Lucianetti, T. Mocek, P. Camy, U. Griebner, V. Petrov, M. Aguiló, F. Díaz, X. Mateos, Monoclinic zinc monotungstate Yb^{3+},Li^{+}:$ZnWO_4$: Part II. Polarized spectroscopy and laser operation, J. Lumin., *submitted* (2020).
30. M. D. Serrano, J. O. Álvarez-Pérez, C. Zaldo, J. Sanz, I. Sobrados, J. A. Alonso, C. Cascales, M. T. Fernández-Díaz, A. Jezowski, Design of Yb^{3+} optical bandwidths by crystallographic modification of disordered calcium niobium gallium laser garnets, J. Mater. Chem. C 5 (2017)11481-11495.
31. Z. Pan, J. M. Serres, E. Kifle, P. Loiko, H. Yuan, X. Dai, H. Cai, M. Aguiló, F. Díaz, Y. Wang, Y. Zhao, U. Griebner, V. Petrov, X. Mateos, Comparative study of the spectroscopic and laser properties of Tm^{3+}, Na^{+}(Li^{+})-codoped $Ca_3Nb_{1.5}Ga_{3.5}O_{12}$-type disordered garnet crystals for mode-locked lasers, Opt. Mater. Express 8 (2018) 2287-2299.
32. F. Yang, C. Tu, Growth and spectroscopy of Ni^{2+} in $ZnWO_4$ crystal, Mater. Lett. 61 (2007) 3056-3058.
33. A. Watterich, M. Wöhlecke, H. Müller, K. Raksányi, A. Breitkopf, B. Zelei, Fe centers and charge compensation in $ZnWO_4$ single crystals characterized by ESR and IR spectroscopy, J. Phys. Chem. Solids 53 (1992) 889-895.
34. F. Yang, C. Tu, J. Li, G. Jia, H. Wang, Y. Wei, Z. You, Z. Zhu, Y. Wang, X. Lu, Growth and optical property of $ZnWO_4$:Er^{3+} crystal, J. Lumin. 126 (2007) 623-628.

35. F. Yang, C. Tu, H. Wang, Y. Wei, Z. You, G. Jia, J. Li, Z. Zhu, X. Lu, Y. Wang, Growth and spectroscopy of Dy^{3+} doped in $ZnWO_4$ crystal, Opt. Mater. 29 (2007) 1861-1865.
36. F. Yang, C. Tu, H. Wang, Y. Wei, Z. You, G. Jia, J. Li, Z. Zhu, X. Lu, Y. Wang, Growth and spectroscopy of $ZnWO_4$:Ho^{3+} crystal, J. Alloys Compd. 455 (2008) 269-273.
37. R. D. Shannon, Revised effective ionic radii and systematic studies of interatomic distances in halides and chalcogenides, Acta Cryst. A 32 (1976) 751-767.
38. N. Onuma, H. Higuchi, H. Wakita, H. Nagasawa, Trace element partition between two pyroxenes and the host lava, Earth Planet Sci Lett 5 (1968) 47–51.
39. G. M. Kuz'micheva, V. B. Rybakov, K. A. Subbotin, E. V. Zharikov, D. A. Lis, O. Zaharko, D. A. Nikolaev, V. G. Senin, Colors of mixed-substituted double molybdate single crystals having scheelite structure, Russ. J. Inorg. Chem. 57 (2012) 1128-1133 [transl. from Zhurnal Neorganicheskoi Khimii 57 (2012) 1205–1211].
40. M. Kuz'micheva, D. A. Lis, K. A. Subbotin, V. B. Rybakov, E. V. Zharikov, Growth and structural X-ray investigations of scheelite-like single crystals Er,Ce:$NaLa(MoO_4)_2$ and Yb:$NaGd(WO_4)_2$, J. Cryst. Growth 275 (2005) e1835–e1842.
41. V. Volkov, M. Rico, A. Méndez-Blas, C. Zaldo, Preparation and properties of disordered $NaBi(XO_4)_2$, X = W or Mo, crystals doped with rare earths, J. Phys. Chem. Solids 63 (2002) 95-105.
42. S.C. Sabharwal, Role of non-stoichiometry in the cracking of oxide crystals, J. Cryst. Growth 310 (2008) 2899-2905.
43. M. G. Brik, V. Nagirnyi, M. Kirm, Ab-initio studies of the electronic and optical properties of $ZnWO_4$ and $CdWO_4$ single crystals, Mater. Chem. Phys. 134 (2012) 1113-1120.
44. R. Lacomba-Perales, J. Ruiz-Fuertes, D. Errandonea, D. Martínez-García, A. Segura, Optical absorption of divalent metal tungstates: correlation between the band-gap energy and the cation ionic radius, Europhys. Lett. 83 (2008) 37002.
45. S. O'hara, Zinc tungstate crystal growth, dislocations, and crystallography, J. Appl. Phys. 35 (1964) 1312-1316.
46. I. Földvári, R. Capelletti, Á. Péter, I. Cravero, A. Watterich, Spectroscopic properties of $ZnWO_4$:Fe single crystals, Solid State Commun. 9 (1986) 855-860.
47. L. F. Bencs, K. Raksányi, O. Szakács, L. Kovács, A. Watterich, Á. Péter, Removal of iron, chromium and sodium impurities from zinc tungstate ($ZnWO_4$), J. Cryst. Growth 181 (1997) 455-458.
48. A. Kornylo, A. Jankowska-Frydel, B. Kuklinski, M. Grinberg, N. Krutiak, Z. Moroz, M. Pashkowsky, Spectroscopic properties of $ZnWO_4$ single crystal doped with Fe and Li impurities, Radiat. Meas. 38 (2004) 707-710.
49. H. Wang, F. D. Medina, M. S. Antonious, C. Párkányi, J. E. Haky, D. M. Baird, Y. D. Zhou, Spectroscopic studies of $ZnWO_4$ single crystals, Chem. Phys. Lett. 205 (1993) 497-501.
50. Z. Kowalski, S. M. Kaczmarek, M. Berkowski, M. Głowacki, Y.A. Zhydachevskii, A. Suchocki, Growth and optical properties of $ZnWO_4$ single crystals pure and doped with Ca and Eu, J. Cryst. Growth 457 (2017) 117-121.
51. O.F. Schirmer, O^- bound small polarons in oxide materials, J. Phys. Cond. Matter 18 (2006) R667.
52. P. F. Schofield, K. S. Knight, S. A. T. Redfern, G. Cressey, Distortion characteristics across the structural phase transition in $(Cu_{1-x}Zn_x)WO_4$, Acta Cryst. B: Struct. Sci. 53 (1997) 102-112.

53. S. C. Sabharwal, Investigations on cracking in $CdWO_4$ crystals, J. Cryst. Growth 216 (2000) 535-537.
54. T. C. Damen, S. P. S. Porto, B. Tell, Raman effect in zinc oxide, Phys. Rev. 142 (1966) 570.
55. Y. Liu, H. Wang, G. Chen, Y. D. Zhou, B. Y. Gu, B. Q. Hu, Analysis of Raman spectra of $ZnWO_4$ single crystals, J. Appl. Phys. 64 (1988) 4651-4653.
56. H. Wang, F. D. Medina, Y. D. Zhou, Q. N. Zhang, Temperature dependence of the polarized Raman spectra of $ZnWO_4$ single crystals, Phys. Rev. B 45 (1992) 10356-10362.
57. A. A. Kaminskii, H. J. Eichler, K. Ueda, N. V. Klassen, B. S. Redkin, L. E. Li, J. Findeisen, D. Jaque, J. García-Sole, J. Fernández, R. Balda, Properties of Nd^{3+}-doped and undoped tetragonal $PbWO_4$, $NaY(WO_4)_2$, $CaWO_4$, and undoped monoclinic $ZnWO_4$ and $CdWO_4$ as laser-active and stimulated Raman scattering-active crystals, Appl. Opt. 38 (1999) 4533-4547.

List of figure captions

Figure 1. Photograph of the as-grown 5 at.% Yb^{3+}, 5 at.% Li^{+}:$ZnWO_4$ crystal (nominal composition): (a-c) Pt/Rh crucible, ZnO (#1) and WO_3 (#2) batches, (a) as-grown boule; (b) central part oriented by means of single-crystal XRD; (c) thick (t = 5 mm) plate cut orthogonal to the growth direction. The growth direction is along the [100] axis; (d) Pt crucible, ZnO (#1) and WO_3 (#2) batches.

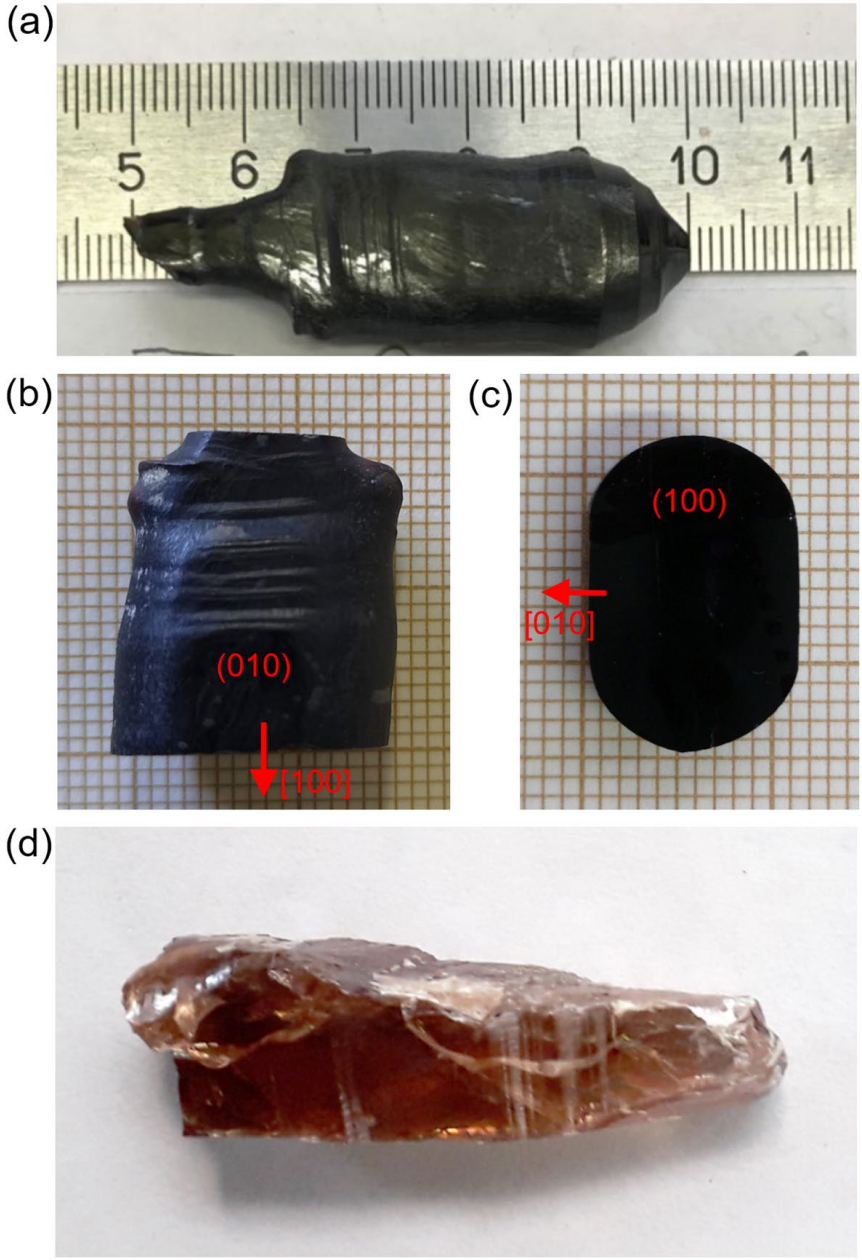

Figure 2. Segregation coefficients of transition-metal (TM) and rare-earth (RE) ions in monoclinic $ZnWO_4$ *vs*. their ionic radius for VI-fold oxygen coordination: this work (*blue squares*) and literature data (*red circles*) [23,29-34]. *Curve*: parabolic fit of the data according to the Onuma's principle, $K_D = 1 - C(R_D - R_{Zn})^2$, $C = 35 \pm 3$ Å^{-2}.

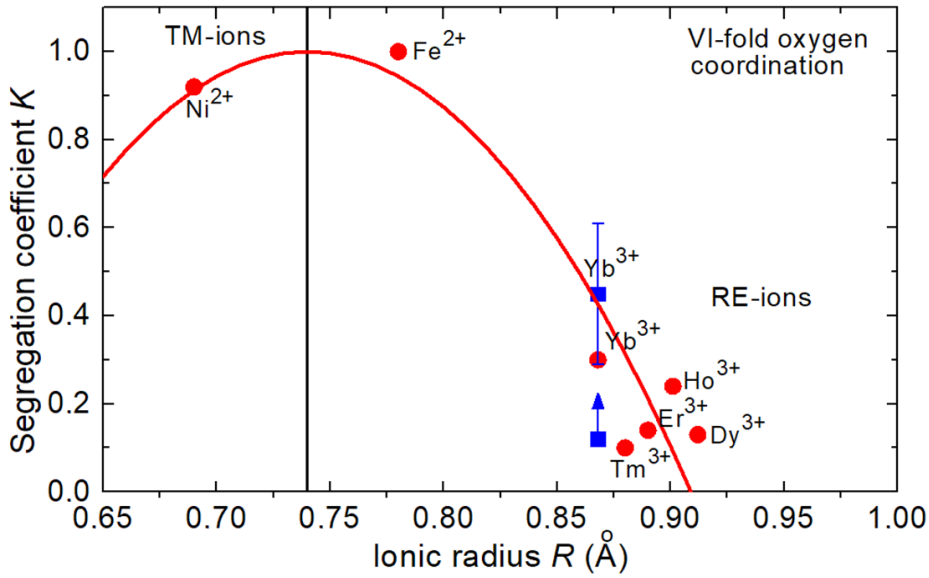

Figure 3. Unpolarized absorption spectra of Yb^{3+},Li^+:$ZnWO_4$ crystals (nominal composition) at RT (293 K) grown using different ZnO and WO_3 reagents.

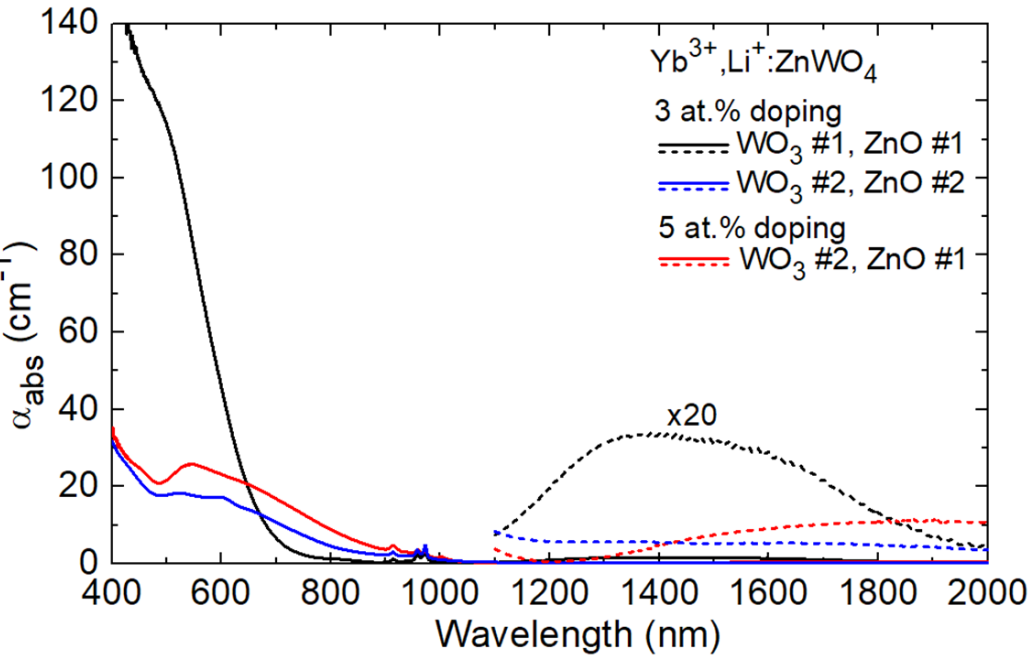

Figure 4. Effect of oxidizing annealing on the unpolarized absorption spectra of $ZnWO_4$ crystals at RT (293 K): (a) 5 at.% Yb^{3+}, 5 at.% Li^+:$ZnWO_4$ (nominal composition) grown using the ZnO (#1) and WO_3 (#2) reagents, annealing at 800 °C for 3 weeks; (b) undoped $ZnWO_4$ grown using the ZnO (#2) and WO_3 (#2) reagents, annealing at 800 °C for 3 weeks; (c) 5 at.% Yb^{3+}, 5 at.% Li^+:$ZnWO_4$ (nominal composition) grown using the ZnO (#1) and WO_3 (#2) reagents and annealed at 800 °C for 24 h or for 3 weeks. *t* – sample thickness. *Inset*: (a) photograph of the thinner crystal plates before (*lower*) and after (*upper*) the annealing, (c) photograph of the crystal plates before (*left*) and after (*right*) the annealing at 800 °C for 24 h.

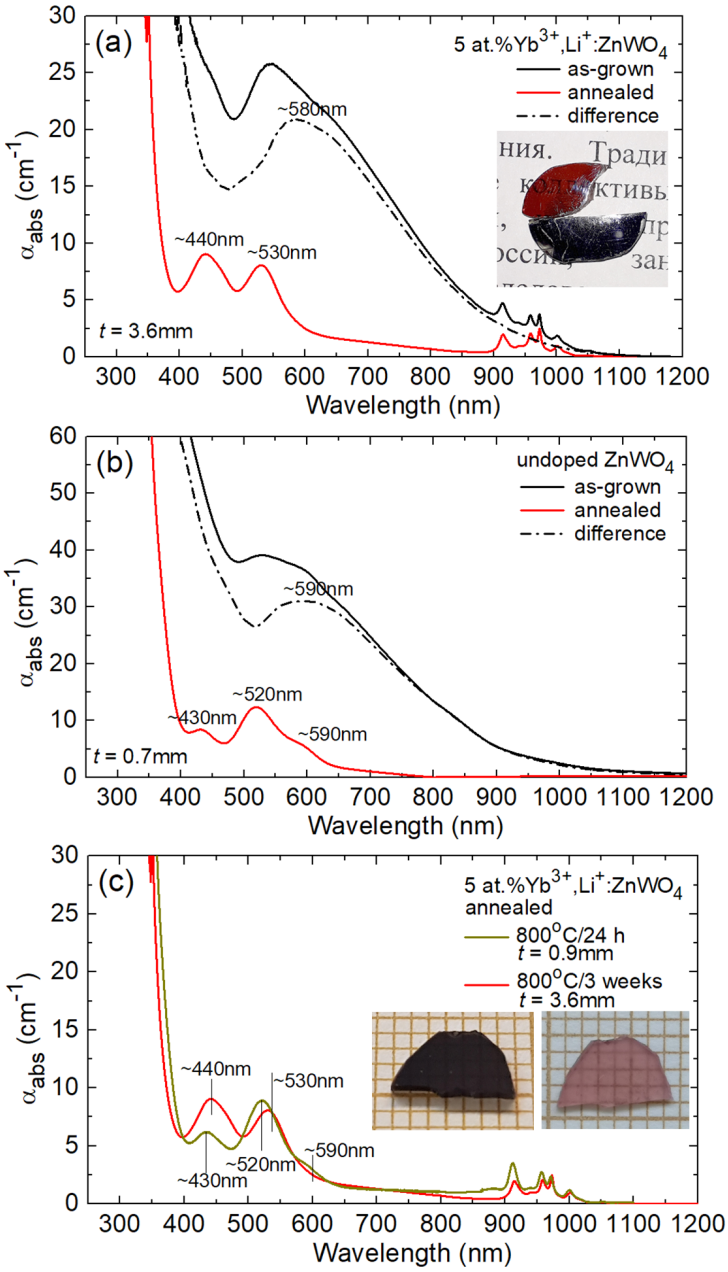

Figure 5. Unpolarized absorption spectrum at RT (293 K) of a 5 at.% Yb^{3+}, 5 at.% Li^{+}:$ZnWO_4$ crystal (nominal composition) grown in a Pt crucible using the ZnO (#1) and WO_3 (#2) reagents, before and after the annealing at 800 °C for 3 weeks. *Inset*: photo of the polished sample (t = 2.9 mm).

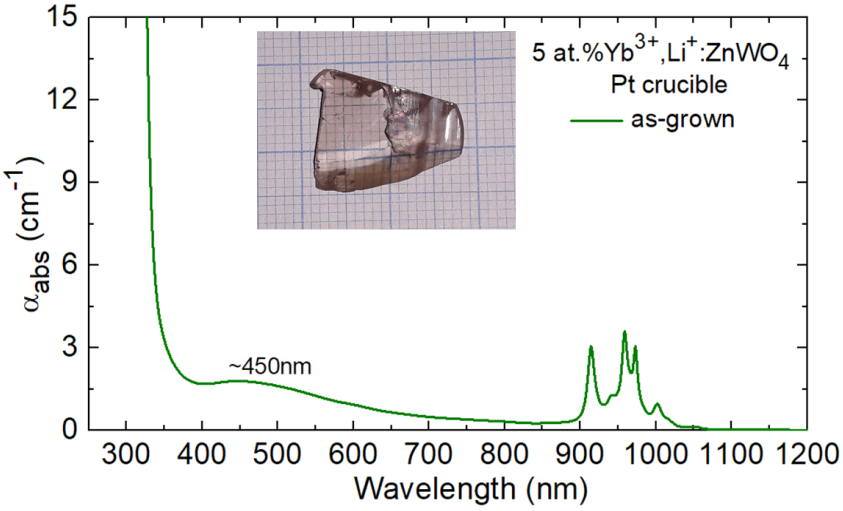

Figure 6. Differential thermal analysis (DTA) curves for the 5 at.% Yb^{3+}, 5 at.% Li^{+}:$ZnWO_4$ crystal (nominal composition).

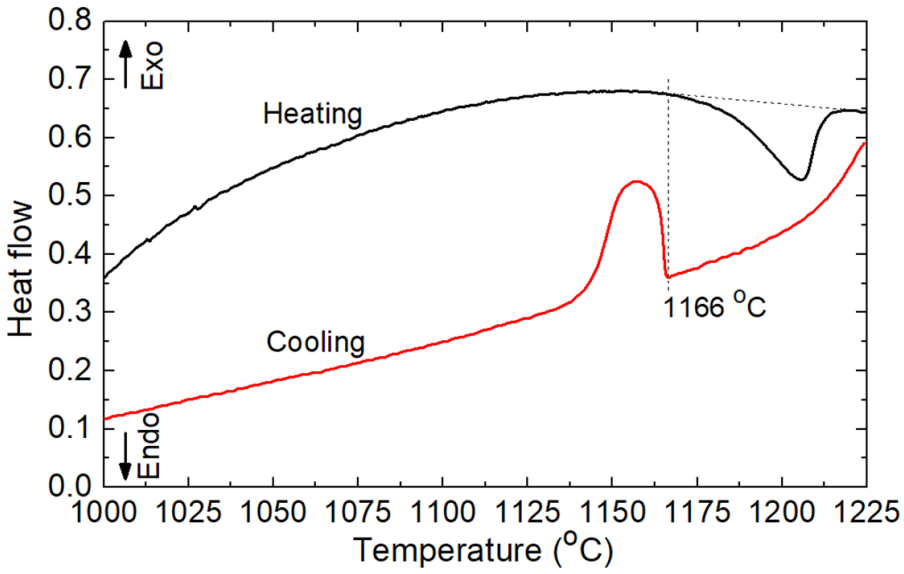

Figure 7. RT X-ray powder diffraction (XRD) pattern of the as-grown 5 at.% Yb^{3+}, 5 at.% Li^{+}:$ZnWO_4$ crystal (nominal composition); the theoretical pattern of undoped $ZnWO_4$ is shown for comparison, JCPDS card #96-210-1676, *numbers* indicate the Miller's indices, (*hkl*).

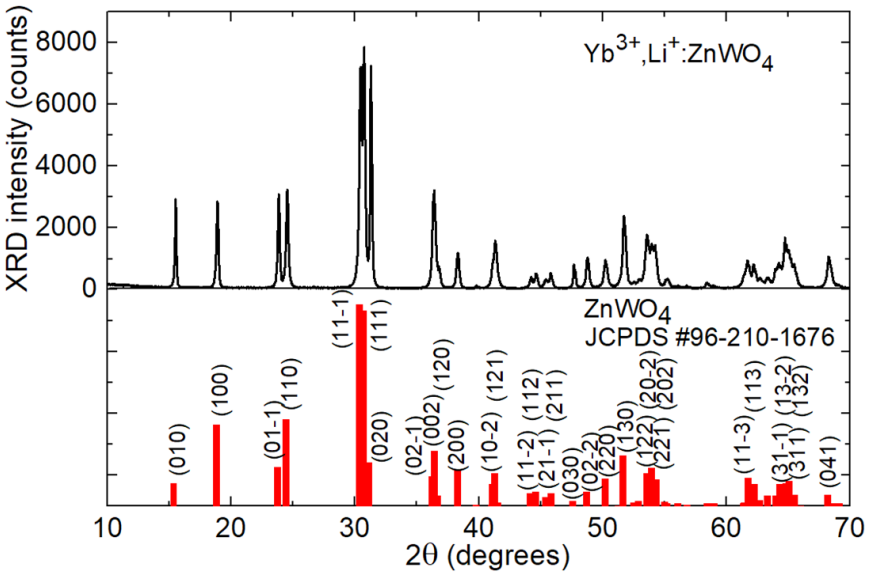

Figure 8. Results of the Rietveld refinement of the RT X-ray powder diffraction (XRD) pattern of the as-grown $Zn_{0.964}Yb_{0.018}Li_{0.018}WO_4$ crystal.

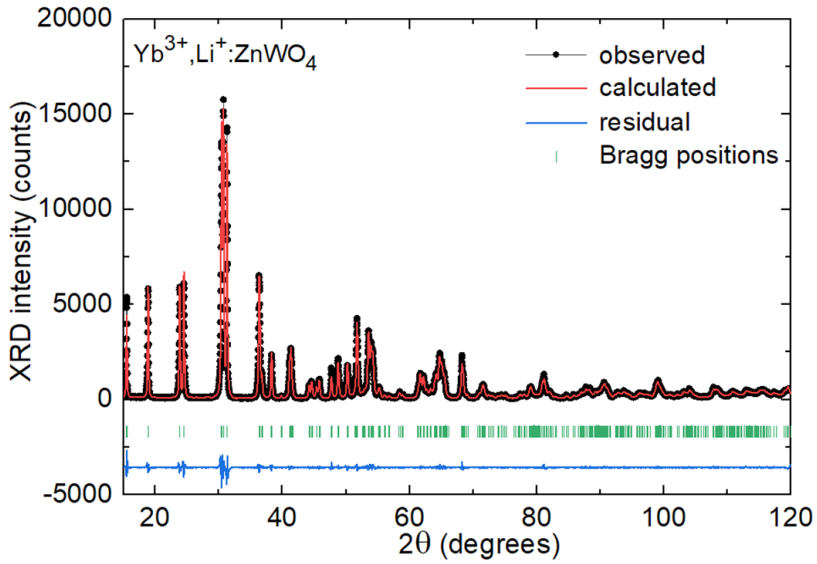

Figure 9. Fragment of crystal structure of Yb^{3+}-doped $ZnWO_4$: (a) projection in the ***b*-*c*** plane; (b) projection in the ***a*-*b*** plane. *Black lines* indicate the unit-cell.

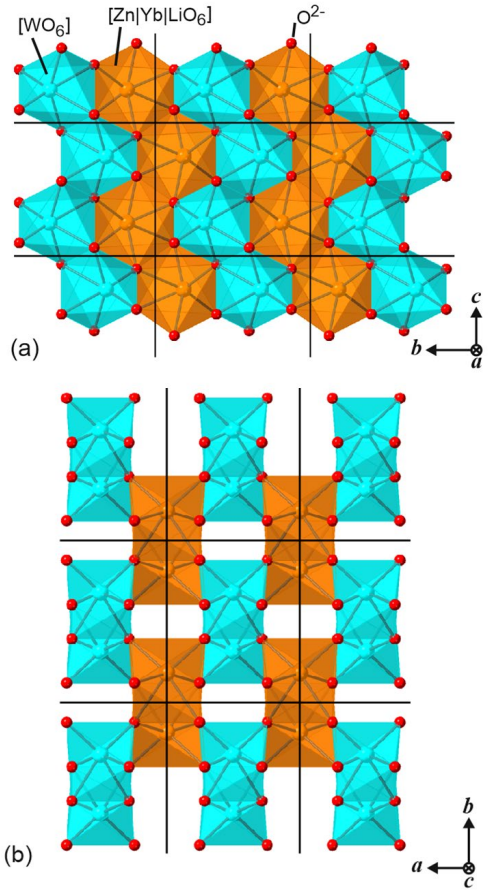

Figure 10. Nearest-neighbor coordination of (a) tungsten and (b) zinc | ytterbium | lithium cations in the monoclinic Yb^{3+},Li^{+}:$ZnWO_4$ crystal.

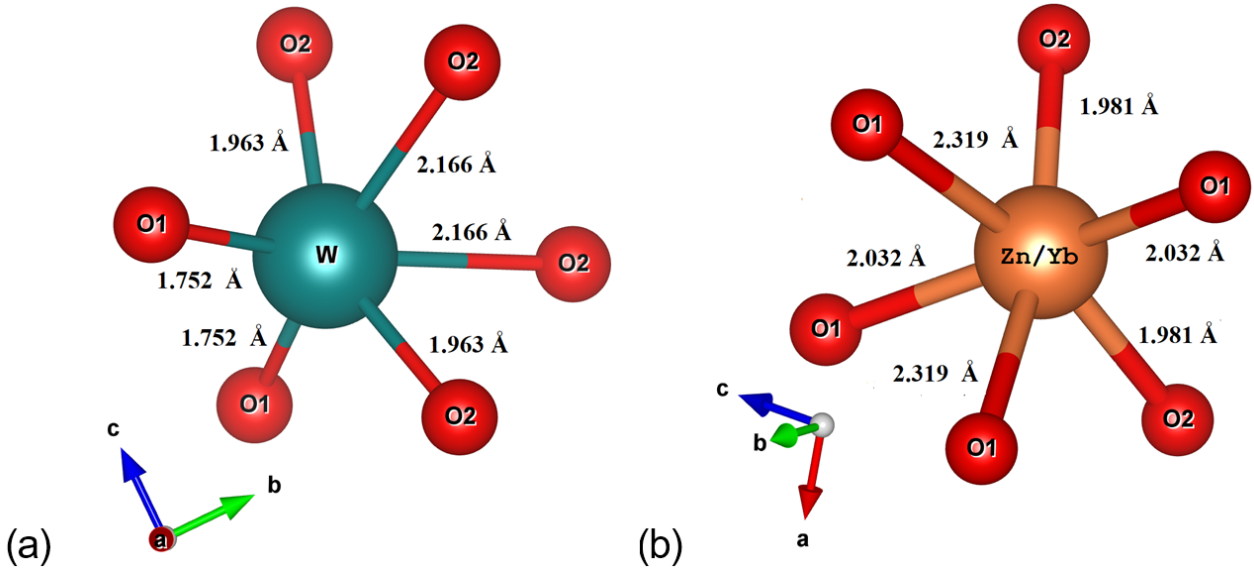

Figure 11. Temperature evolution of the unit-cell parameters (L = a, b, c and c*) of 5 at.% Yb^{3+}, 5 at.% Li^{+}:$ZnWO_4$ (nominal composition) according to the data of high-temperature XRD.

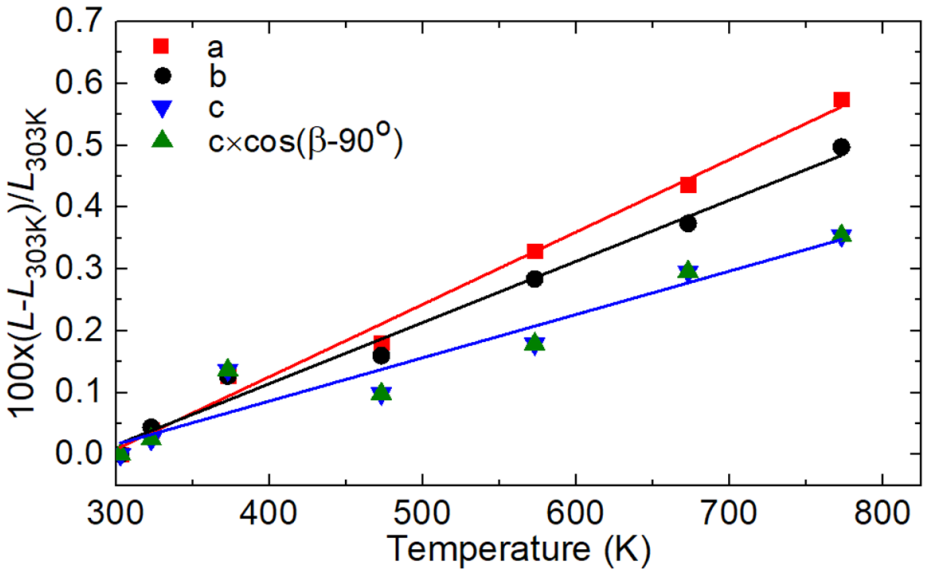

Figure 12. Mutual orientation of the crystallographic axes (***a***, ***b***, ***c***) and principal axes of the thermal expansion tensor (X'_1, X'_2, X'_3) in Yb^{3+},Li^{+}:$ZnWO_4$.

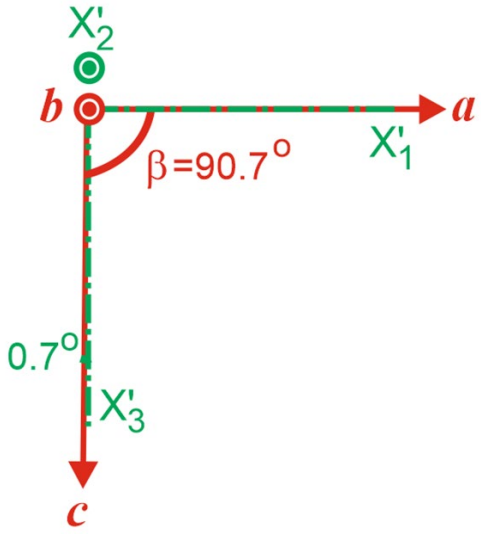

Figure 13. Polarized Raman spectra of the as-grown 5 at.% Yb^{3+}, 5 at.% Li^{+}:$ZnWO_4$ crystal (nominal composition) for the (a) $a(ij)\bar{a}$, (b) $b(ij)\bar{b}$ and (c) $c(ij)\bar{c}$ geometries (Porto's notations). The *numbers* indicate the frequencies of Raman bands in cm^{-1}. λ_{exc} = 514 nm.

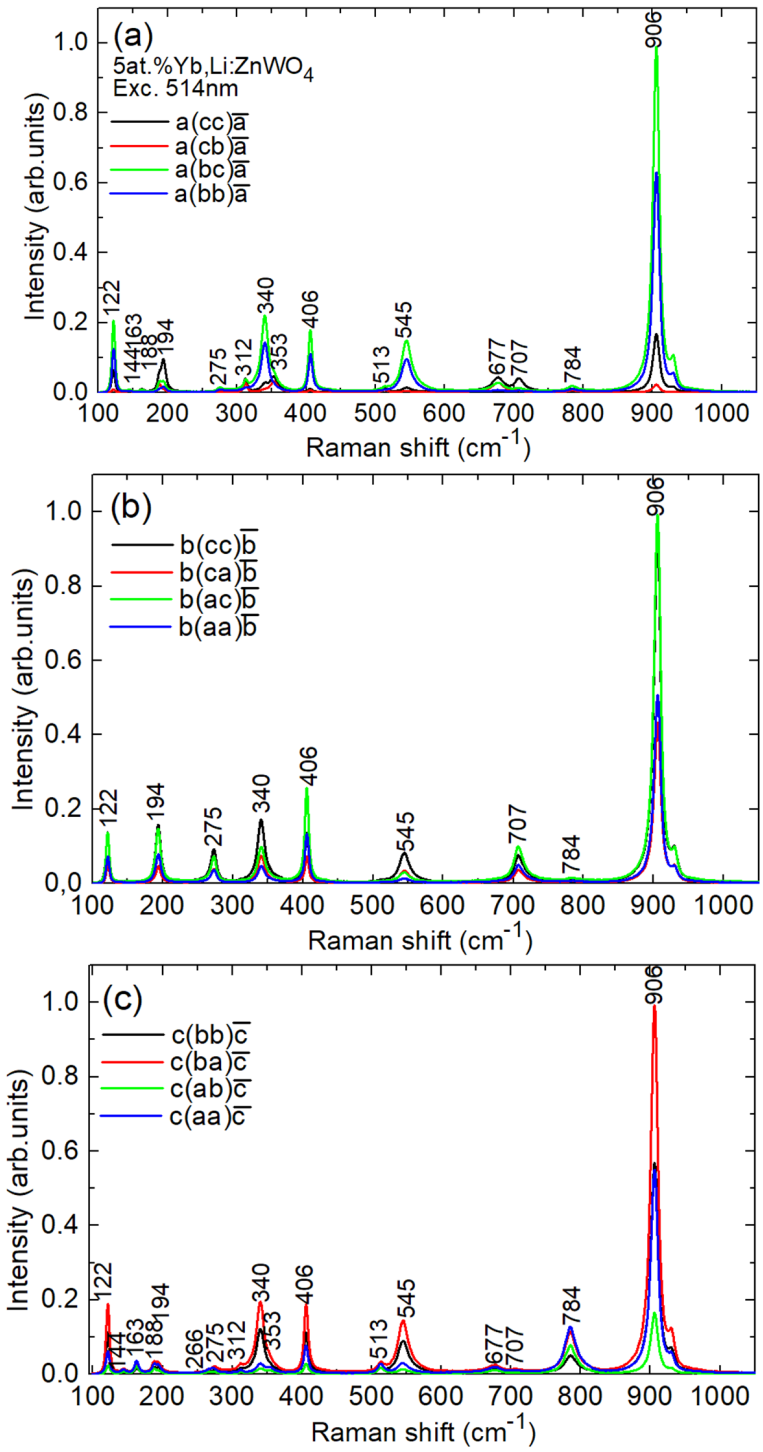

Table 1. Results of the impurity compositional analysis of the as-grown zinc tungstate crystals: 3 at.% Yb^{3+}, 3 at.% Li^{+}:$ZnWO_4$ (nominal composition; reagents: ZnO (#1) and WO_3 (#1)) and undoped $ZnWO_4$ (reagents: ZnO (#2) and WO_3 (#2)) by the SSMS method.

Element	ppm, weight		Element	ppm, weight	
	Yb^{3+},Li^{+}:$ZnWO_4$	$ZnWO_4$		Yb^{3+},Li^{+}:$ZnWO_4$	$ZnWO_4$
Li	*20*	*0.8*	*Zn*	*host-forming*	
O	*host-forming*		Zr	<0.05	<0.05
Na	0.6	20	**Nb**	**40**	**10**
Mg	2	6	**Mo**	**10**	**60**
Si	20	10	Ru	<0.1	<0.1
Cl	800	1000	**Rh**	**40**	**80**
K	0.4	2	Cd	2	<0.1
Ca	2	30	In	<0.1	<0.1
Sc	0.2	0.2	Sn	<0.1	<0.1
Ti	<0.01	<0.01	Er	<0.1	<0.1
V	0.4	<0.01	Tm	<0.1	<0.1
Cr	**9**	**10**	*Yb*	*>2000*	*20*
Mn	**8**	**6**	*W*	*host-forming*	
Fe	**200**	**50**	Re	<0.2	<0.2
Co	<0.02	<0.02	Os	<0.2	<0.2
Ni	**20**	**2**	Ir	<0.2	<0.2
Cu	**2**	**20**	Pt	<0.2	<0.2

Table 2. Parameters of the Rietveld refinement of the structure of the as-grown $Zn_{0.964}Yb_{0.018}Li_{0.018}WO_4$ crystal.

Parameters	Values
System	Monoclinic
Space group	$P2/c$ – C^4_{2h}
Laue class	$2/m$
Space group IT number	13
Lattice constants (a – b – c) (Å)	4.702(2) – 5.718(6) – 4.930(4)
Angles α – β – γ (deg)	90 – 90.713(5) – 90
Cell volume V_{calc} (Å^3)	132.571
Number of the formula units Z	2
Crystal density ρ_{calc} (g/cm^3)	7.553
2θ range (deg)	14.5–120
Radiation	Cu-Kα1 (λ = 1.5406 Å)
No. of reflections	399
No. of points	5270
Background Parameters – No.	Linear interpolation – 72
Refinement	Rietveld (FullProf)
Reliability factors	R_p = 8.11, R_{wp} = 11.6, χ^2 = 7.03, R_b = 0.89, R_f = 0.38

Table 3. Fractional atomic coordinates (x, y, z), occupancy factors (O.F.) and isotropic displacement parameters (B_{iso}) of the as-grown $Zn_{0.964}Yb_{0.018}Li_{0.018}WO_4$ crystal.

Atom	Site	x	y	z	B_{iso}	O.F.
Zn	2e	1/2	0.687(8)	1/4	0.978	0.964
Yb	2e	1/2	0.687(8)	1/4	0.978	0.018
Li	2e	1/2	0.687(8)	1/4	0.978	0.018
W	2f	0	0.189(9)	1/4	0.552	1
O1	4g	0.256(4)	0.365(0)	0.412(0)	1.513	1
O2	4g	0.220(8)	0.894(2)	0.429(0)	1.722	1

Table 4. Lattice constants of undoped and RE^{3+}-doped $ZnWO_4$ crystals reported so far.

Crystal	*a*, Å	*b*, Å	*c*, Å	*β*, °	Ref.
$ZnWO_4$	4.69263(5)	5.72129(7)	4.92805(5)	90.6321(9)	[7]
$ZnWO_4$	4.6902(1)	5.7169(1)	4.9268(1)	90.626(1)	[28]
Yb^{3+},Li^{+}:$ZnWO_4$	4.702(2)	5.718(6)	4.930(4)	90.713(5)	This work
Eu^{3+},Ca^{2+}:$ZnWO_4$	4.697	5.727	4.938	90.69	[47]

Table 5. Characterization of the $[WO_6]$ and $[(Zn|Yb|Li)O_6]$ polyhedra in the 5 at.% Yb^{3+}, 5 at.% Li^{+}:$ZnWO_4$ crystal (nominal composition).

Polyhedron	$[WO_6]$	$[(Zn|Yb)O_6]$
Interatomic distances	(W-O2) = 2.166(4) ×2	(Zn|Yb-O2) = 1.981(0) ×2
M – O, Å	(W-O2) = 1.963(4) ×2	(Zn|Yb-O1) = 2.032(9) ×2
	(W-O1) = 1.752(2) ×2	(Zn|Yb-O1) = 2.319(5) ×2
Average bond length, Å	1.9607	2.1112
Polyhedral volume, $Å^3$	9.5065	12.1496
Distortion index (bond length)	0.07089	0.06581
Quadratic elongation	1.0455	1.0267
Bond angle variance, $deg.^2$	128.863	73.8797
Effective coordination number	4.0237	4.9634

Table 6. Thermal expansion coefficients for $M^{2+}WO_4$ crystals reported so far.

Crystal	*α*, 10^{-6} K^{-1}			Method*	Ref.
	[100]	[010]	[001]		
Cr^{3+}:$MgWO_4$	10.5	15.7	10.8	DIL	[14]
Ho^{3+}:$MgWO_4$	11.22	8.09	8.77	XRD	[5]
$CdWO_4$	6.39	10.9	6.45	DIL	[49]
$ZnWO_4$	9.64	8.63	6.45	DIL	[4]
Yb^{3+},Li^{+}:$ZnWO_4$	11.71	9.90	7.01	XRD	This work

*XRD – high-temperature XRD, DIL – dilatometry.

Table 7. Raman-active modes observed in Yb^{3+},Li^{+}:$ZnWO_4$ (at RT).

No.	Frequency, cm^{-1}		Symmetry	Internal mode
	Yb^{3+},Li^{+}:$ZnWO_4$	$ZnWO_4$ [55]		
1	906	906.8	A_g	+
2	784	785.9	B_g	+
3	707	709.1	A_g	+
4	677	678.7	B_g	
5	545	546.4	A_g	
6	513	515.3	B_g	
7	406	406.9	A_g	+
8	353	355.4	B_g	
9	340	341.8	A_g	+
10	312	314.6	B_g	
11	275	274.4	A_g	
12	266	267.3	B_g	
13	194	195.3	A_g	
14	188	190.0	B_g	+
15	163	164.5	B_g	
16	144	146.3	B_g	
17	122	123.2	A_g	
18	–	91.5	B_g	